Enhanced Light Out-Coupling in Organic Light-Emitting Diodes by Patterning the Cathode in Graded Photonic Super-crystals

Safaa Hassan [1], David Lowell [1] and Yuankun Lin [1,2]
[1] Department of Physics, University of North Texas, Denton, TX 76203, USA;
SafaaHassan@my.unt.edu; DavidLowell@my.unt.edu; yuankun.lin@unt.edu
[2] Department of Electrical Engineering, University of North Texas, Denton, TX 76203, USA

1. ABSTRACT

Coupling of light to surface plasmons at metal cathode represents a significant light loss in organic light-emitting diode. The newly discovered graded photonic super-crystals with dual periodicity and dual basis, present great opportunity to improve the light out-coupling (The light extraction efficiency) from organic light-emitting diodes. These graded photonic super-crystals can be holographically fabricated by eight beam interference lithography. In this paper, we have computed, through electrodynamic simulation, the light extraction efficiency of planar, organic light-emitting diodes where the Al cathode is patterned with the graded photonic super-crystals. When the cathode of an organic light-emitting device is patterned in the graded photonic super-crystals, a light extraction efficiency up to 70% in the visible range can be achieved.

Keywords: photonic crystals; graded photonic super-crystals; holographic lithography; extraction efficiency; organic light emitting device; spatial light modulator

2. INTRODUCTION

Using photonic crystals for the integration of functional optical devices, photonic band gap engineering, and enhanced light–matter interactions has been extensively studied [1–2]. The traditional periodic photonic crystals (PhCs) with a single basis have uniform lattices [3], as shown inside the solid red square in Figure 1. Second-generation periodic PhCs have dual lattices with one set of lattices [4-5], the dual lattices indicated by the black and yellow dots in Figure 1 where the Second-generation of photonic crystals have greatly enhanced broadband light absorption when integrated with light-absorptive [4-5]. Future-generation PhCs [here called graded photonic super-crystals (GPSCs) have superlattices with dual periodicity, dual symmetry, and dual basis and a graded filling fraction of dielectric material [6-10]. They are called GPSCs due to a large unit super-cell in the PhC and gradient basis in the unit super-cell. Very recently, we have demonstrated direct holographic fabrication of graded, superlattice PhCs with dual periodicity, dual symmetry, and dual basis, using a spatial light modulator (SLM) [6-10].

The lattices are grouped by the black and yellow dots. However, the size of the basis is different in GPSC as shown in Figure 1. The basis size is the gradient, becoming smaller along the arrows for both blue and red lattice sets in Figure 1, and then becoming larger after a quarter of period. The unit cell becomes a unit super-cell in the GPSC, as opposed to the dual lattice in the second-generation photonic crystals. The first period is the period for the traditional photonic crystal, while second period is the second period in the x-direction for the GPSC, as shown in Figure 1. The lattice described by fiest period has a square symmetry, while the lattice described by the second period can have square, five-fold symmetry, or hexagonal [6–10]. Thus, the GPSC can have dual-symmetries and dual-periods. The lattice with first period can have other symmetries, with a cost of reduced resolution in a phase pattern if a spatial light modulator (SLM) is used in the fabrication [6–10]. The filling fraction of the dielectric material in the GPSC is also the gradient for the regions where the dashed red square region has a high filling fraction and the solid red square region has a low filling fraction.

On the other hand, the organic light-emitting diodes (OLED) have been extensively studied for many applications [11-14]. Coupling of light to surface plasmons at metal cathode represents a significant light loss in organic light-emitting diode. Some external out-coupling structures such as shaped substrate and micro-lenses have been used to improve the out-couple efficiency in the substrates for OLEDs [15-19]. One of the important ways which have been used to improve the light extraction efficiency for OLEDs is using the 2D photonic crystals (PhCs) as one type of internal light extraction structure for LEDs. By incorporating internal light extraction structures between OLED layers and substrates or in the active layer, the light out-coupling efficiency for planar OLEDs can be improved [20-21].

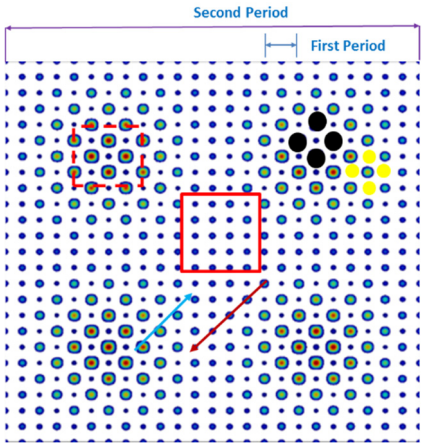

Figure 1. Image of photonic super-crystals: the lattices can be grouped by black and yellow dots. The size of the basis becomes smaller along the blue and red arrows, and then becomes larger after a quarter of "Period 2".

In this paper, we study the extraction efficiency and of light from the organic light emitting device, by using the graded photonic super-crystals (GPSCs) with a rectangular unit super-cell. By texturing the cathode of the white OLED with graded superlattice PhCs with dual basis, the highest light extraction efficiency into glass substrate has been predicted by simulation.

3. PATTERNING WITH GRADED SUPERLATTICE PHOTONIC CRYSTALS

Two sets of interfering beams are used (4-beam for each), where the total eight beams are overlapped form a pattern. The E is the electric field for these eight beams given by the following equations:

$$\mathbf{E_1}(r,t) = \boldsymbol{E}_1 \cos[+(k\sin\alpha_1\, cos45)x + (k\sin\alpha_1\, sin45)y + (k\cos\alpha_1)z - \omega t + \phi_1] \quad (1)$$

$$\mathbf{E_2}(r,t) = \boldsymbol{E}_2 \cos[-(k\sin\alpha_1\, cos45)x + (k\sin\alpha_1\, sin45)y + (k\cos\alpha_1)z - \omega t + \phi_2] \quad (2)$$

$$\mathbf{E}_3(r,t) = \boldsymbol{E}_3 \cos[-(k\sin\alpha_1\, cos45)x - (k\sin\alpha_1\, sin45)y + (k\cos\alpha_1)z - \omega t + \phi_3] \quad (3)$$

$$\mathbf{E_4}(r,t) = \boldsymbol{E}_4 \cos[+(k\sin\alpha_1\, cos45)x - (k\sin\alpha_1\, sin45)y + (k\cos\alpha_1)z - \omega t + \phi_4] \quad (4)$$

$$\mathbf{E_5}(r,t) = \boldsymbol{E}_5 \cos[+(k\sin\alpha_2\, cos\beta)x + (k\sin\alpha_2\, sin\beta)y + (k\cos\alpha_2)z - \omega t + \phi_5] \quad (5)$$

$$\mathbf{E_6}(r,t) = \boldsymbol{E}_6 \cos[-(k\sin\alpha_2\, cos\beta)x + (k\sin\alpha_2\, sin\beta)y + (k\cos\alpha_2)z - \omega t + \phi_6] \quad (6)$$

$$\mathbf{E_7}(r,t) = \boldsymbol{E}_7 \cos[-(k\sin\alpha_2\, cos\beta)x - (k\sin\alpha_2\, sin\beta)y + (k\cos\alpha_2)z - \omega t + \phi_7] \quad (7)$$

$$\mathbf{E_8}(r,t) = \boldsymbol{E}_8 \cos[+(k\sin\theta_2\, cos\beta)x - (k\sin\theta_2\, sin\beta)y + (k\cos\alpha_2)z - \omega t + \phi_8] \quad (8)$$

Where E is the electric field; k is the wave vector; α_1 and α_2 (zenith angle) are the interfering angles of the two sets of beams (outer and inner beams), respectively; β and 45° are the azimuthal angles for inner and outer beams, respectively; and ϕ is the initial phase of the beam. When the eight beams are overlapped, the intensity distribution in the interference pattern is determined by the following:

$$I(r) = \langle \sum_{i=1}^{8} E_i^2(r,t) \rangle + \sum_{i<j}^{8} \boldsymbol{E}_i \cdot \boldsymbol{E}_j \cos\left[\left(k_j - k_i\right) \cdot r + \left(\phi_j - \phi_i\right)\right]. \quad (9)$$

The nine (Equations 1–9) were programed in MATLAB, which produced interference patterns with one example in Figure 2b. The eight-beam interference can also be approximately understood by adding the interference of beams 1–4 and beams 5–8. The inference of beams 1–4 forms a structure with a small period of $\Lambda_s = 2\pi/(k\sin(\alpha_1)\cos(45))$. The period

Λ_x in x-direction in the interference among beams 5-8 is different from period Λ_y in the y-direction, and are calculated as follows: $\Lambda_x = 2\pi/(k \sin(\alpha_2) \cos(\beta))$ and $\Lambda_y = 2\pi/(k \sin(\alpha_2) \sin(\beta))$.

A simulated eight-beam interference pattern, as shown in Figure 2b, assumes the same initial phase for all eight beams in Equation (9). The periodicity in the x- and y-directions (Λ_x, Λ_y) is labeled for the size of the unit super-cell.

Although both the rectangular (6 × 12) and square (12 × 12) sub-unit cells are used, the sub-unit cell, as indicated by the dashed green line, is in a rectangular shape in Figure 2b. The unit super-cell in Figure 2b has a ratio of length over width of $\Lambda_y/\Lambda_x = 24/18$, which is obtained from (12 + 12)/ (12 + 6). The design of the phase pattern is flexible for obtaining a rectangular unit super-cell in a holographic structure.

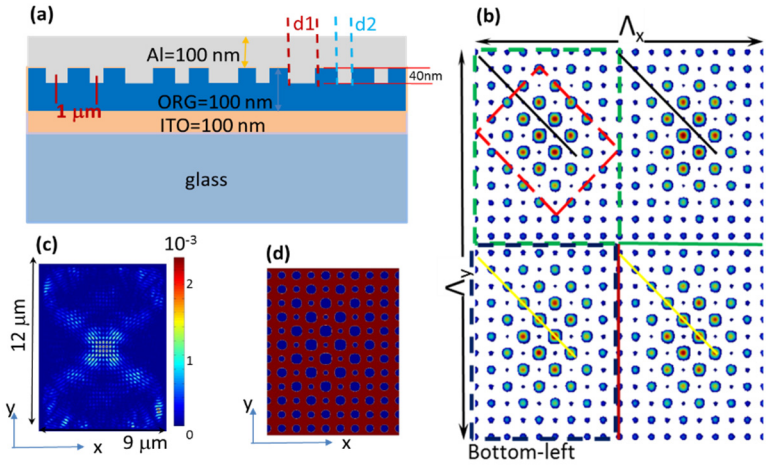

Figure 2. (**a**) Schematic of the organic light emitting device (OLED) where the cathode (Al) is patterned with the graded photonic super-crystal that has a rectangular unit super-cell; (**b**) Simulated eight-beam interference pattern.; (**c**) electric-field intensity in the glass substrate in OLED at the location 740 nm away from indium tin oxide (ITO) layer; (**d**) output of the structure design from the simulation software MIT Electromagnetic Equation Propagation (MEEP).

4. ELECTRODYNAMIC SIMULATIONS OF LIGHT EXTRACTION EFFICIENCY

In this section, we simulated the light extraction efficiency in the organic light emitting device (OLED) by using the MIT Electromagnetic Equation Propagation MEEP (an open-source finite-difference time-domain (FDTD)) simulation tool [22], where the cathode is patterned with the graded photonic super-crystal with the rectangular unit super-cell. Due to the large unit super-cell (12 × 9 times larger than the one in the traditional photonic crystal), we performed parallel simulations using the Simpetus Electromagnetic Simulation Platform in Amazon Web Services (AWS). The E-field intensity was monitored, as shown in Figure 2c for example, in the glass substrate in OLED. In this simulation, a lattice period (small period) of 1 μm is used, as shown in Figure 2a. The 100 nm organic-layer (ORG) includes the light emitting layer, the hole transport layer, and electron transport layer. We assigned refractive indices n for the glass (n = 1.45), organic (n = 1.8), and indium tin oxide (ITO) (n = 1.8) layers [7,21]. Ten different incoherent electric point-dipole sources were placed along a vertical line in the center of the ORG layer and dipoles with different polarization directions are assigned [21].

The interference of eight-beam pattern in Figure 2b can be divided into four sections. The top two sections have a low-intensity lattice set starting from the top-left corner of each section, indicated by the black lines. The bottom two sections have a high-intensity lattice set starting from the corner, as indicated by the yellow lines. The simulation results should be the same if we select the whole one or a quarter of unit super-cell, based on our experience [7,8,10]. One case for the simulation of different sections, described in Figure 2, is from the literature [8]. To save the computation time, a quarter of the unit super-cell (bottom left section in Figure 2b) was used in the simulation. Figure 2d shows a permittivity structure output from the MEEP tool with a sub-unit cell size of 9a × 12a (a = 1000 nm). The E-field intensity was monitored, as shown in Figure 2c for example, in the glass substrate in OLED. The fraction of the total power as a function of the wavelength can be obtained for the light in the glass substrate, light absorbed by Al cathode (in plasmonic mode), and trapped as a waveguide mode, as shown in Figure 3a-d.

The light intensity in air in fraction is 6.6% less than that in the glass substrate, as simulated for other structures [10]. However, the simulation of the extraction efficiency into the glass substrate takes much less time. To save the computation time and focus on the fabrication effect, we simulated the extraction efficiency into the glass substrate for OLED, where the cathode (Al) is patterned with the graded photonic super-crystal formed under different exposure thresholds. Figure 3 shows the percentage of light in the glass substrate over the total power as a function of the wavelengths for the rectangular sub-unit, as shown in Figure 2d. The light exposure thresholds of 25%, 30%, and 35% of the maximum intensity I_{max} were used in the simulations.

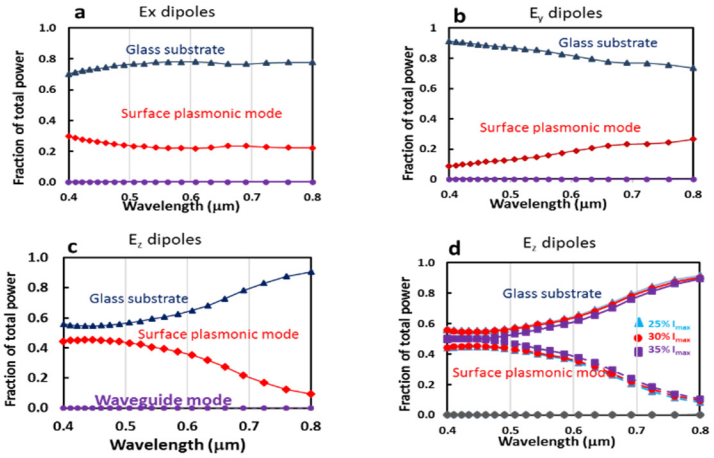

Figure 3. Fraction of the total emitted power in glass substrate, both in the surface plasmonic mode and in the waveguide as a function of the wavelengths for exposure threshold 30% I_{max} for the E_x dipoles (a), E_y dipoles (b), E_z dipoles (c), and E_z dipoles for different exposure thresholds of 25% I_{max}, 30% I_{max}, and 35% I_{max} (d).

The results for the dipole polarization of E in the y-, x-, and z-directions are shown in Figure 3a–c, respectively. Overall, the extraction efficiency is between 70% and 80% for the dipole polarization in the xy plane. The extraction efficiency is 86.6% for the E_y dipoles for the 30% I_{max} threshold, while they are 76.6% for the E_x dipoles at 524 nm. It is reasonable, because the graded intensity is modulated in a higher number of steps along a length of the rectangle in the y-direction, rather than the x-direction. The extraction efficiency for the Ez dipoles in Figure 3d is not significantly dependent on the exposure threshold, as the groove depth of 40 nm in Figure 3a is fixed in the simulation. All parameters used in the simulations in Figure 3 are the same as the graded photonic super-crystal with a square super-unit [8], where the maximum efficiency for the E_z dipoles occurred at 400 or 760 nm. The maximum efficiency of the E_z dipoles in Figure 3 was in the infrared range beyond 800 nm.

An overall light extraction efficiency, φ, can be calculated using the average efficiency of the dipoles polarized in x–y (parallel dipole) and z (perpendicular dipole) [7,21], as follows:

$$\varphi = \frac{2}{3}\varphi_{x-y} + \frac{1}{3}\varphi_z \quad (10)$$

Where the ρ_{x-y} and ρ_z are also the average efficiency for ten dipoles. The extraction efficiency is calculated to be 71% at 563 nm and 73% at 633 nm. For all of the exposure threshold conditions, the lowest extraction efficiency is 65% at 434 nm in the visible range. The high-light extraction efficiency can be understood through the effective light coupling condition provided by the graded photonic super-crystals in Equation (11) [23], as follows:

$$\frac{2\pi}{\lambda} n_{eff} - \frac{2\pi}{\lambda}\sin(\alpha) = R \quad (11)$$

where n_{eff} is the effective refractive index of the graded photonic super-crystal, λ is the wavelength in free space, and R is the reciprocal lattice vector. The effective refractive index is related to the filling fraction f by Equation (12), as follows:

$$n_{eff} = \sqrt{n_{metal}^2(1-f) + n_{org}^2 f} \quad (12)$$

where n_{metal} and n_{org} are the refractive index of the metal and organic material in the graded photonic super-crystal, respectively. Because of the graded filling fraction in graded photonic super-crystals (GPSCs), the coupling condition can be met by many wavelengths simultaneously. The wavelength-dependent plasmonic loss is depended on the size of the basis at the lattice of the graded photonic super-crystal (GPSCs) [24]. When the sizes of the basis at neighboring lattices are different, as shown in Figure 2a (d1 and d2), the plasmonic resonance condition is destroyed, thus less plasmonic loss can be seen in the simulation.

5. CONCLUSIONS

In conclusion, we have explored the superior capability of improving the light extraction efficiency of OLEDs using graded photonic super-crystals with a rectangular unit super-cell. Where the eight-beam interference can provide flexible design for the graded photonic super-crystals with a different ratio of length over the width of the rectangular unit super-cell. The light extraction efficiency has been computed in three regions: glass substrate, organic/metal interface, and planar organic/ITO layer for OLEDs with the Al cathode patterned with the graded super-lattice. The enhancement of extraction efficiency has been explained in term of surface plasmon resonance and verified by E-field intensity distributions. A large light extraction efficiency up to 70% into glass substrate has been predicted through simulation, where the high extraction efficiency is maintained for different exposure thresholds during the interference lithography.

Acknowledgement: This research was funded by U.S. National Science Foundation, grant number 1661842.

REFERENCES

[1] Tandaechanurat, A.; Ishida, S.; Guimard, D.; Nomura, M.; Iwamoto, S.; Arakawa, Y.," Lasing oscillation in a three-dimensional photonic crystal nanocavity with a complete bandgap," Nat. Photonics, 5, 91–94 (2011).

[2] Ergin, T.; Stenger, N.; Brenner, P.; Pendry, J.B.; Wegener, M.," Three-dimensional invisibility cloak at optical wavelengths," Science, 328, 337–339 (2010).

[3] Joannopoulos, J.D.; Villeneuve, P.R.; Fan, S.H. Photonic crystals: Putting a new twist on light. Nature, 386, 143–149 (1997).

[4] Rinnerbauer, V.; Shen, Y.; Joannopoulos, J.D.; Soljačić, M.; Schäffler, F.; Celanovic, I.," Superlattice photonic crystal as broadband solar absorber for high temperature operation," Opt. Express, 22, A1895–A1906 (2014).

[5] Rinnerbauer, V.; Lausecker, E.; Schäffler, F.; Reininger, P.; Strasser, G.; Geil, R.D.; Joannopoulos, J.D.; Soljačić, M.; Celanovic, I.," Nanoimprinted superlattice metallic photonic crystal as ultraselective solar absorber," Optica, 2, 743–746 (2015).

[6] Lowell, D.; Lutkenhaus, J.; George, D.; Philipose, U.; Chen, B.; Lin, Y.," Simultaneous direct holographic fabrication of photonic cavity and graded photonic lattice with dual periodicity, dual basis, and dual symmetry," Opt. Express, 25, 14444–14452 (2017).

[7] Hassan, S.; Lowell, D.; Lin, Y.," High light extraction efficiency in organic light-emitting diodes by patterning the cathode in graded superlattice with dual periodicity and dual basis," J. Appl. Phys., 121, 233104 (2017).

[8] Hassan, S.; Lowell, D.; Adewole, M.; George, D.; Zhang, H.; Lin, Y.," Extraordinary light trapping enhancement in silicon solar cell patterned with graded photonic super-crystals," Photonics, 4, 50 (2017).

[9] Lowell, D.; Hassan, S.; Adewole, M.; Philipose, U.; Chen, B.; Lin, Y.," Holographic fabrication of graded photonic super-crystals using an integrated spatial light modulator and reflective optical element laser projection system," Appl. Opt., 56, 9888–9891 (2017).

[10] Lowell, D.; Hassan, S.; Sale, O.; Adewole, M.; Hurley, N.; Philipose, U.; Chen, B.; Lin, Y.," Holographic fabrication of graded photonic super-quasi-crystal with multiple level gradients," Appl. Opt., 57, 6598–6604 (2018).

[11] Kido, J.; Hongawa, K.; Nagai, K., "White light-emitting organic electroluminescent devices using the poly(N-vinylcarbazole) emitter layer doped with three fluorescent dyes," Appl. Phys. Lett. 64, 815 (1994)

[12] Baldo, M. A.; O'Brien, D. F.; You, Y.; Shoustikov, A.; Sibley, S.; Thompson, M. E.; Forrest, S. R.," Highly efficient phosphorescent emission from organic electroluminescent devices," Nature, 395, 6698, 151-154 (1998).

[13] Bhansali, U.; Polikarpov, E.; Swensen, J.S.; Chen, W.; Jia, H.; Gaspar, D.J.; Gnade, B.E.; Padmaperuma, A.B.; Omary, M.A., "High-efficiency turquoise-blue electrophosphorescence from a Pt(II)-pyridyltriazolate complex in a phosphine oxide host," Appl. Phys. Lett. 95, 233304 (2009).
[14] Sasabe, H.; Kido, J.," Recent Progress in Phosphorescent Organic Light-Emitting Devices," Eur. J. Org. Chem. 2013, 7653–7663 (2013).
[15] Sun. Y.; Forrest, S.R.," Enhanced light out-coupling of organic light-emitting devices using embedded low-index grids," Nat. Photonics 2(8), 483–487 (2008).
[16] D'Andrade, B.W.; J. J. Brown, J.J.," Organic light-emitting device luminaire for illumination applications,"Appl. Phys. Lett. 88(19), 192908 (2006).
[17] Sun. Y.; Forrest, S.R.," Organic light emitting devices with enhanced outcoupling via microlenses fabricated by imprint lithography," J. Appl. Phys. 100(7), 073106 (2006).
[18] Feng, J.; Okamoto, T.; and Kawata, S.," Highly directional emission via coupled surface-plasmon tunneling from electroluminescence in organic light-emitting devices," Appl. Phys. Lett. 87(24), 241109 (2005).
[19] Chen, C.Y.; Lee, W.K.; Chen, Y.J.; Lu, C.Y.; Lin, H.Y.; Wu, C.C.," Enhancing Optical Out-Coupling of Organic Light-Emitting Devices with Nanostructured Composite Electrodes Consisting of Indium Tin Oxide Nanomesh and Conducting Polymer," Adv. Mater. 27(33), 4883–4888 (2015).
[20] Qu, Y.; Slootsky, M.; Forrest, S.R.," Enhanced light extraction from organic light-emitting devices using a sub-anode grid," Nature Photonics 9, 758–763 (2015).
[21] Oskooi, A.," Texturing the cathode of white organic light-emitting diodes with a lattice of nanoscale scatterers for enhanced light out-coupling," Appl. Phys. Lett., 106, 041111 (2015).
[22] Oskooi, A.F.; Roundy, D.; Ibanescu, M.; Bermel, P.; Joannopoulos, J.D.; and Johnson, S.G.," MEEP: A flexible free-software package for electromagnetic simulations by the FDTD method," Comput. Phys. Commun., 181, 687–702 (2010).
[23] Shi, J.; Pollard, M.E.; Angeles, C.A.; Chen, R.; Gates, J.C.; Charlton, M.D.B.," Photonic crystal and quasi-crystals providing simultaneous light coupling and beam splitting within a low refractive-index slab waveguide," Sci. Rep., 7, 1812 (2017).
[24] Adewole, M.; Lowell, D.; Hassan, S.; George, D.; Zhang, H.; Cui, J.; Lin, Y.," Broadband plasmonic total light absorption in an Al-doped ZnO/spacer/silver stack patterned with graded photonic super-crystal," Res. J. Opt. Photonics, 1, 1 (2017).